Observations of increasing carbon dioxide concentration in Earth's thermosphere

J. T. Emmert[1]*, M. H. Stevens[1], P. F. Bernath[2,3,4], D. P. Drob[1] and C. D. Boone[3]

Carbon dioxide occurs naturally throughout Earth's atmosphere. In the thermosphere, CO_2 is the primary radiative cooling agent and fundamentally affects the energy balance and temperature of this high-altitude atmospheric layer[1,2]. Anthropogenic CO_2 increases are expected to propagate upward throughout the entire atmosphere, which should result in a cooler, more contracted thermosphere[3-5]. This contraction, in turn, will reduce atmospheric drag on satellites and may have adverse consequences for the orbital debris environment that is already unstable[6,7]. However, observed thermospheric mass density trends derived from satellite orbits are generally stronger than model predictions[8,9], indicating that our quantitative understanding of these changes is incomplete. So far, CO_2 trends have been measured only up to 35 km altitude[10-12]. Here, we present direct evidence that CO_2 concentrations in the upper atmosphere—probably the primary driver of long-term thermospheric trends—are increasing. We analyse eight years of CO_2 and carbon monoxide mixing ratios derived from satellite-based solar occultation spectra. After correcting for seasonal–latitudinal and solar influences, we obtain an estimated global increase in CO_x (CO_2 and CO, combined) concentrations of 23.5 ± 6.3 ppm per decade at an altitude of 101 km, about 10 ppm per decade faster than predicted by an upper atmospheric model. We suggest that this discrepancy may explain why the thermospheric density decrease is stronger than expected.

In the mesosphere (50–90 km altitude) and thermosphere (>90 km), almost all carbon is partitioned between CO_2 and CO through ultraviolet photolysis of CO_2 to create CO and chemical loss of CO to re-form CO_2 (refs 1,13). The photochemistry and atmospheric dynamics introduce solar cycle, seasonal and latitudinal dependences into the partitioning and the overall carbon abundance[13,14]. The CO_2 volume mixing ratio (VMR) is approximately constant up to 65–80 km and falls off rapidly at higher altitudes owing to molecular diffusion and photolysis[13]. The proportion of carbon in the form of CO increases from less than 3% below 80 km to more than 20% above 100 km (refs 13,14). CO_2 cools the mesosphere and thermosphere through collisional excitation (by atomic oxygen) of its bending vibrational mode and subsequent 15 μm band emission, most of which escapes from the thin upper atmosphere[1,2].

We analysed temporal changes in CO_2 and CO VMRs measured by the Atmospheric Chemistry Experiment Fourier Transform Spectrometer[15] (ACE-FTS) from April 2004 to September 2011, using the approach described in Methods. Figure 1 shows the CO_2
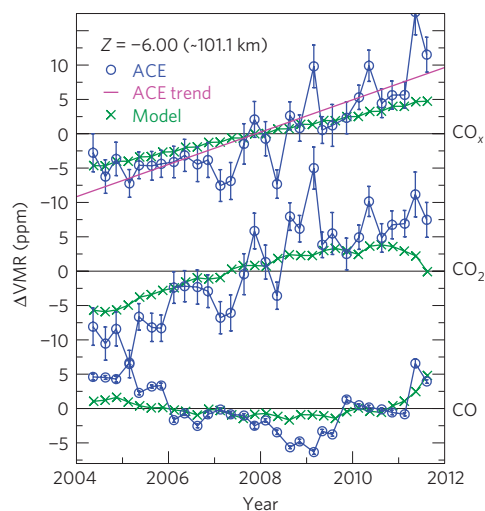
Figure 1 | Residual VMRs of CO, CO_2 and $CO_x = CO + CO_2$, after removal of seasonal–latitudinal effects. Results are shown at pressure level $Z = -6$ (altitude ~101 km) for ACE-FTS (blue circles) and the NCAR global mean model (green crosses). The solid pink line is the linear trend from a least-squares fit of the ACE-FTS CO_x residuals. Error bars denote the estimated 1σ uncertainty of the mean.

and CO residual time series, after removal of seasonal–latitudinal variations and the overall mean, at a pressure level corresponding to an altitude of ~101 km. Also shown is a corresponding analysis of the combined CO_2 and CO VMRs, which we term CO_x. As expected from photochemistry, the CO VMR varies in phase with the solar cycle (with a minimum in 2008–2009), whereas the CO_2 increase is attenuated during the 2009–2012 ascending phase of the solar cycle. The CO_x VMR, however, increases fairly steadily from 2004 to 2012, with a least-squares linear trend of 23.5 ± 6.3 ppm per decade, where the uncertainty is the 95% confidence interval. As the partitioning of carbon between CO and CO_2 is influenced primarily by solar ultraviolet irradiance, the trend in CO_x should be largely free of solar cycle variations and thus can be used to estimate the long-term relative trend in CO_2, assuming the relative proportion of CO and CO_2 is stable.

For comparison with the ACE-FTS trends, we conducted simulations with the National Center for Atmospheric Research (NCAR) global mean model of the mesosphere, thermosphere and ionosphere[1]. We conducted a 1992–2012 global mean model

[1]Space Science Division, Naval Research Laboratory, 4555 Overlook Avenue Southwest, Washington DC 20375, USA, [2]Department of Chemistry and Biochemistry, Old Dominion University, 5115 Hampton Boulevard, Norfolk, Virginia 23529, USA, [3]Department of Chemistry, University of Waterloo, 200 University Avenue, West Waterloo, Ontario N2L 3G1, Canada, [4]Department of Chemistry, University of York, Heslington, York YO10 5DD, UK.
*e-mail: john.emmert@nrl.navy.mil.
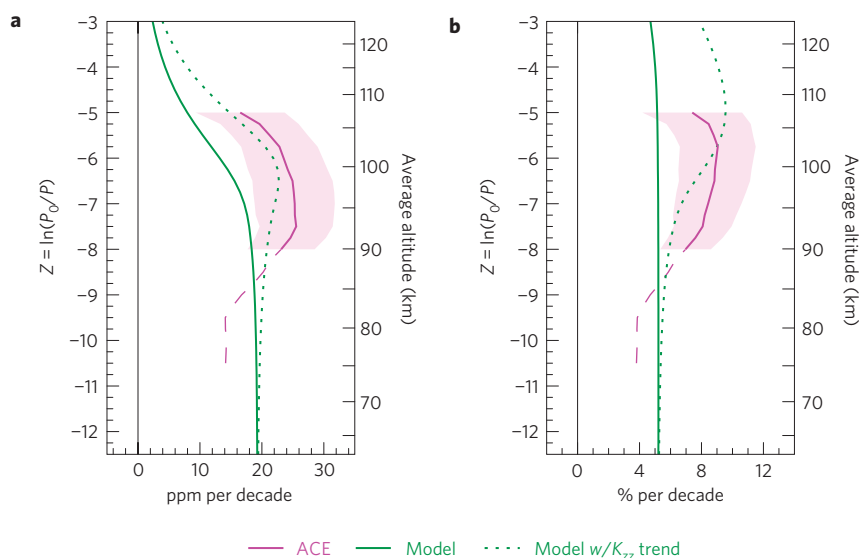
Figure 2 | Height dependence of 2004–2012 CO_x linear trends. a, Absolute trends. **b**, Relative trends, obtained by dividing the absolute trends by the profiles shown in Fig. 4. Results are shown for ACE-FTS (pink), the NCAR global mean model (solid green) and the global mean model with a 15% per decade eddy diffusion trend added (dotted green). The shaded areas encompass the estimated 95% confidence interval of the ACE-FTS trends. The dashed lines denote the portion of the ACE-FTS trend profiles that is influenced by the prescribed stratospheric CO_2 trends.

simulation using interpolated annual global mean CO_2 VMRs measured in the troposphere[16] to specify CO_2 variations at the model's lower boundary of 30 km, and we repeated the ACE-FTS analysis procedure on the 2004.25–2012.75 daily output of the model simulation. The model CO_x residual time series is shown in Fig. 1, and exhibits a noticeably weaker trend (13.2 ± 0.3 ppm per decade) than the ACE-FTS data. Figure 2a shows height profiles (computed on a pressure grid as described in Methods) of the CO_x linear trends. The ACE-FTS trends between 90 and 105 km decrease with increasing altitude at approximately the same rate as the model trends, but the ACE-FTS trends are 5–10 ppm per decade larger than the model trends. Figure 2b shows the relative trends (that is, normalized to the average CO_x VMR), which are approximately constant with height between 90 and 105 km: ~8% per decade for ACE-FTS, ~5% per decade for the global mean model.

In Fig. 2, the decrease in the ACE-FTS trends below 90 km is probably an artefact of the retrieval process, which specifies the CO_2 VMR a priori below ~70 km and transitions to free retrieval at higher altitudes[17]. The imposed stratospheric trend of 15 ppm per decade is based on 1980s and 1990s tropospheric CO_2 data; the observed tropospheric trend averaged ~20 ppm per decade during the 2000s. We tested the effect of using the more realistic stratospheric trend by reprocessing a subset of the ACE-FTS occultations; the measured trend above 90 km changed by less than 1.5 ppm per decade, which is well within the statistical uncertainty of 6.3 ppm per decade. We also fitted the global mean model CO_2 profiles to the ACE-FTS CO_2 retrieval function and found that the model trends above 90 km are uninfluenced by the stratospheric constraint.

Figure 3 shows the 1992–2012 temporal variation of CO_2, CO and CO_x VMRs from the model simulation at 101 km. The solar cycle amplitude of CO_x is less than 1 ppm, which is much smaller than the expected decadal CO_2 increase of >10 ppm and supports our use of CO_x trends as a proxy for long-term CO_2 trends. However, Fig. 1 indicates that the solar cycle dependence is stronger in the ACE-FTS data than in the model, so the model's representation of solar influences is probably incomplete.

Figure 4 shows average absolute profiles of CO_2, CO and CO_x VMRs from the model and from ACE-FTS for 2004.25–2011.75.
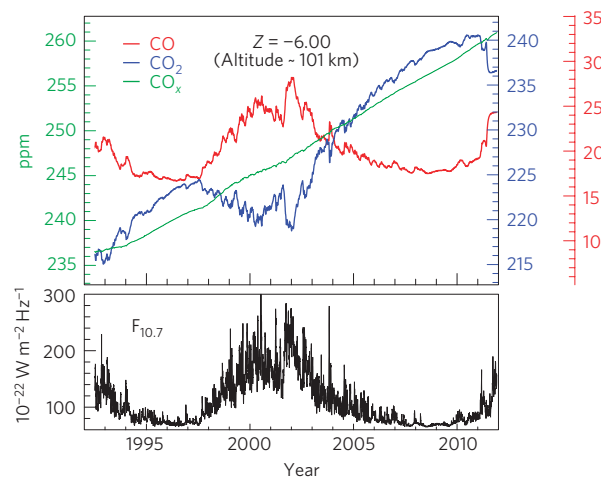
Figure 3 | Temporal variation of carbon at pressure level $Z = -6$ (altitude ~101 km) from the NCAR global mean model simulation. Shown are VMRs of CO (red), CO_2 (blue) and $CO_x = CO + CO_2$ (green). The data are plotted according to the colour-coordinated y axes. The bottom panel shows the 10.7 cm solar radio flux ($F_{10.7}$), a proxy for solar ultraviolet irradiance.

The CO_2 VMR begins to fall off above ~80 km in the data and above ~95 km in the model. There are long-standing discrepancies between measured and modelled CO_2 profiles, particularly with respect to the height of departure from a well-mixed state (the knee; refs 13,14). Models also generally underestimate the CO VMR in the mesosphere and lower thermosphere[13], although good agreement was obtained[14] between the ACE-FTS data and the Canadian Middle Atmosphere Model. Our comparisons (Figs 1 and 2) between data and model temporal changes should not be significantly affected by the discrepancies in the baseline profiles.

The 10 ppm per decade difference between the ACE-FTS and global mean model CO_x trends in the 90–105 km altitude region is statistically significant at the 95% level. The discrepancy suggests that previous simulations of long-term thermospheric density and temperature trends[3,18,19] may have underestimated the enhanced cooling and contraction of the thermosphere attributable to
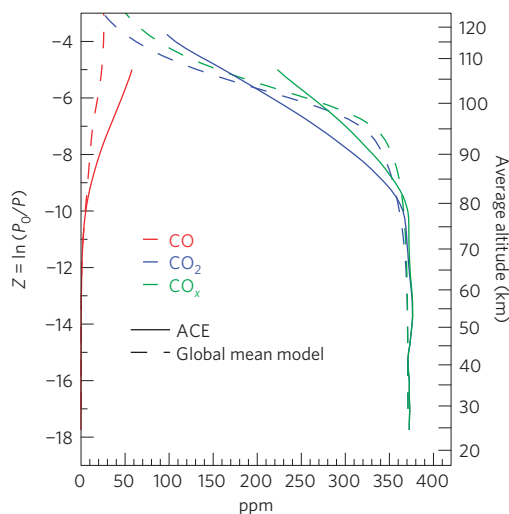
Figure 4 | Average carbon profiles. 2004–2012 average CO (red), CO_2 (blue) and CO_x (green) VMR profiles, from ACE (solid lines) and the NCAR global mean model (dashed lines).

anthropogenic carbon emissions, because they used CO_2 trends from the global mean model or assumed vertically uniform relative trends. The larger observed CO_2 trends may therefore explain the larger observed thermospheric density decrease[8]. Below, we consider several possible explanations for an elevated lower thermospheric CO_2 trend.

The ACE-FTS trends are not a true global average, because the data represent only sunrise and sunset conditions and are weighted towards high latitudes. When the sunrise and sunset data are treated separately, the difference in trends is negligible, suggesting that there is not a strong local time dependence to the trends. There does seem to be a preference towards larger trends at lower latitudes and under high-latitude summer conditions, but those features are not statistically significant in our analysis.

A trend in atmospheric dynamics (including gravity wave activity[20] and stratospheric mean meridional circulation[21]) could potentially increase vertical mixing and advective transport, which, because of the negative gradient of the CO_2 (and CO_x) VMR above 80 km (Fig. 4), would enhance the carbon trend in this region. There is some observational evidence that mesospheric gravity wave activity is increasing, at least in selected regions[20]. In the global mean model, the eddy diffusion parameter serves as a proxy for vertical mixing and advective transport; by default it has a fixed vertical profile. Imposing a trend in eddy diffusion of +15% per decade (in addition to the tropospheric CO_2 trend) produces a model CO_x trend that is close to the observed ACE-FTS trend (Fig. 2).

A positive trend in eddy diffusion would also contribute to the anomalously low thermospheric mass densities during the 2008–2009 solar minimum[22]. The extra CO_2 drawn up from the lower mesosphere would enhance the cooling and contraction of the thermosphere, and increased downward diffusion would lower the concentration of atomic oxygen in the upper thermosphere (where it is the dominant species), thereby reducing the mass density at a fixed height. In ref. 22 it was estimated that the anomalously low densities were caused by a 14 K reduction in exospheric temperature and a 12% depletion of atomic oxygen density in the lower thermosphere, compared with the previous solar minimum after accounting for the inter-minima change in solar irradiance and geomagnetic activity. In comparison, the combination of the CO_2 and eddy diffusion trends imposed on the global mean model produces an inter-minima exospheric temperature change of 3 K and a change of O density of 17%. Thus, these mechanisms seem to provide a plausible explanation for both the ACE-FTS CO_2 trends

and the anomalously low density of lower thermospheric O inferred from satellite drag measurements.

More detailed investigation of the regional effects and the contribution of atmospheric dynamics to CO_2 trends in the lower thermosphere will require the use of whole-atmosphere general circulation models.

In addition to tropospheric releases, another potential source of excess carbon in the upper atmosphere is *in situ* injection from the exhaust of orbital launch vehicles. For this source to contribute significantly to carbon trends, the rate of its downward diffusion must be slower than the rate of deposition, and a long-term increase in the deposition rate is probably also necessary. From the number and type of rocket launches between 2004 and 2012 (refs 23,24) we estimate a deposition of 2,700 metric tons of carbon above 90 km. In comparison, the difference between the ACE-FTS and model CO_x trends between 90 and 105 km amounts to an extra 20,000 tons of carbon between 2004 and 2012. Therefore, even in the highly unlikely event that all of the carbon from space traffic exhaust has remained resident in the lower thermosphere, it cannot account for the difference between the ACE-FTS trends and the global mean model trends.

Finally, we note that the ACE-FTS CO_2 retrievals consider only the ground vibrational state, to minimize non-local thermodynamic equilibrium effects. At a kinetic temperature of 200 K (typical of the 90–105 km region), approximately 1.6% of the CO_2 population is in the excited bending state (see Supplementary Methods). A trend in the partitioning among the ground and vibrationally excited states could alias as a trend in the retrieved CO_2, although it is unlikely that such an effect could explain the 10 ppm per decade difference between the ACE-FTS and global mean model trends. However, the excited states can in principle be derived from the FTS spectra, which would clarify this issue. Better knowledge of the population of each state would also illuminate the interactions among vertical mixing (which increases CO_2 in the mesosphere and lower thermosphere and decreases lower thermospheric O), atomic oxygen (the primary exciter of the CO_2 vibrational states), CO_2 (the primary cooling agent of the mesosphere and thermosphere) and solar ultraviolet irradiance (which photolyses CO_2 and O_2 and may drive variations in vertical mixing).

Methods

ACE was launched in 2003 into a 74° circular orbit at an altitude of 650 km. The FTS measures high-resolution absorption spectra, covering wavelengths from 2.3 μm to 13.3 μm, during occultations of the Sun by the Earth's limb. From these spectra, height profiles of temperature, pressure and the concentrations of more than thirty species (including CO_2 and CO) are retrieved. Supplementary Fig. S1 shows the latitude dependence of ACE-FTS sunrise and sunset occultations as a function of day of year. Most profiles are measured at mid to high latitudes. The sampling pattern approximately repeats from year to year, owing to the 123-day orbital precession period of ACE. This sampling consistency allows us to remove the seasonal–latitude dependence of CO_2 and CO from the data, and thereby isolate the longer-term trends.

For this study, we used version 3.0 ACE-FTS retrievals of temperature, pressure and CO_2 (ref. 14). The retrievals above 65 km use small (typically 0.4 cm^{-1} wide) regions of the CO_2 spectrum that have minimal interference from other molecules and contain spectral lines originating in the ground vibrational state[14,17]. The CO_2 VMR is prescribed a priori between ~25 and 60–75 km altitude; at higher altitudes, the retrieval transitions smoothly to an unconstrained, simultaneous estimation of CO_2 VMR and temperature[14,17]. The prescribed stratospheric CO_2 VMR includes a trend of 15 ppm per decade (ref. 17), and the influence of the imposed trends extends upward through the transition region, so the data can be used to estimate trends independently only in the lower thermosphere (above ~90 km).

For CO, we used a recently developed retrieval algorithm. The high-altitude portion of the CO retrievals employs a set of 22 lines in the CO fundamental band spanning the wavenumber range 2081–2187 cm^{-1}, with an upper altitude of 110 km for the retrievals. Version 3.0 CO retrievals suffered problems from the assumed shape of the CO VMR profile above the highest analysed measurement: the CO VMR profile was assumed to increase rapidly with increasing altitude above 110 km, but this was inconsistent with observed CO lines in ACE-FTS spectra above 110 km. In contrast, the research product used in our analysis employed a constant CO VMR profile above the highest analysed measurement. This profile shape gives

significantly improved agreement between measured and calculated CO lines above 110 km (that is, above the altitude range employed in the CO retrieval) compared with the version 3.0 results.

We analysed ~26,500 ACE-FTS profiles from April 2004 to September 2011, using data records in which temperature and pressure were retrieved, rather than specified a priori. We excluded data from the first three months of 2004 because of spacecraft pointing problems during this early part of the mission. We first converted the profiles, which are given in geodetic altitude, to a pressure grid $Z = \ln(P_0/P)$, where $P_0 = 5 \times 10^{-7}$ hPa. We then determined the seasonal–latitude dependence of the data along the sampling paths shown in Supplementary Fig. S1, by binning and averaging the data in 48 day-of-year bins (bin width 7.6 days) and treating sunrise and sunset data separately (an example is shown in Supplementary Fig. S2). Measurements more than two standard deviations away from the initial averages were omitted from the final binned average calculations. The seasonal–latitude patterns are highly consistent from year to year. We subtracted the binned averages from the VMR data in the corresponding bins to obtain a set of residuals that is nominally free of seasonal–latitude variations. We combined the sunrise and sunset residuals and averaged them in 3-month bins (excluding outliers more than two standard deviations from the initial average) to obtain a 7.5-year series of 30 average residual profiles. We estimated ACE CO_x trends and their uncertainty from the time series of 3-month averages, following the method described in ref. 25, which accounts for correlated errors describable by autoregressive processes of arbitrary order (see Supplementary Methods for further information on error sources and uncertainty estimation).

The NCAR global mean model[1] solves the one-dimensional energy, vertical diffusion and photochemical equations governing the upper atmosphere. The lower boundary of the model, where the input CO_2 VMR is specified, is at $Z = -17$ (~30 km altitude). Using version 1.2 of the model, we conducted a 1992–2012 simulation using interpolated annual global mean CO_2 VMRs measured in the troposphere[16] (http://www.esrl.noaa.gov/gmd/ccgg/trends/global.html) to specify lower boundary CO_2 variations. We added a constant offset of −13 ppm to the tropospheric time series to obtain a lower boundary CO_2 VMR of 372 ppm at epoch 2008.5, to approximately match the 2004–2011 ACE-FTS average at 30 km. The simulation includes solar ultraviolet irradiance and geomagnetic activity variations as parameterized by the 10.7 cm solar radio flux ($F_{10.7}$) and the Ap index, respectively.

References

1. Roble, R. G. Energetics of the mesosphere and thermosphere. *Geophys. Monogr. Ser.* **87,** 1–21 (1995).
2. Mlynczak, M. G. *et al.* Observations of infrared radiative cooling in the thermosphere on daily to multiyear timescales from the TIMED/SABER instrument. *J. Geophys Res.* **115,** A03309 (2010).
3. Roble, R. G. & Dickinson, R. E. How will changes in carbon dioxide and methane modify the mean structure of the mesosphere and thermosphere? *Geophys. Res. Lett.* **16,** 1441–1444 (1989).
4. Laštovička, J. *et al.* Emerging pattern of global change in the upper atmosphere and ionosphere. *Ann. Geophys.* **26,** 1255–1268 (2008).
5. Qian, L., Laštovička, J., Roble, R. G. & Solomon, S. C. Progress in observations and simulations of global change in the upper atmosphere. *J. Geophys Res.* **116,** A00H03 (2011).
6. Lewis, H. G., Saunders, A., Swinerd, G. & Newland, R. J. Effect of thermospheric contraction on remediation of the near-Earth space debris environment. *J. Geophys Res.* **116,** A00H08 (2011).
7. Liou, J-C. & Johnson, N. L. Instability of the present LEO satellite populations. *Adv. Space Res.* **41,** 1046–1053 (2008).
8. Emmert, J. T., Picone, J. M. & Meier, R. R. Thermospheric global average density trends, 1967–2007, derived from orbits of 5000 near-Earth objects. *Geophys. Res. Lett.* **35,** L05101 (2008).
9. Cnossen, I. in *Greenhouse Gases—Emission, Measurement and Management* (ed. Liu, G.) 315–336 (InTech, 2012); available at http://www.intechopen. com/books/greenhouse-gases-emission-measurement-and-management/ climate-change-in-the-upper-atmosphere.
10. Keeling, R. F., Piper, S. C., Bollenbacher, A. F. & Walker, J. S. *Trends: A Compendium of Data on Global Change. Carbon Dioxide Information Analysis Center* (Oak Ridge National Laboratory, 2009).
11. Bischof, W., Borchers, R., Fabian, P. & Krüger, B. C. Increased concentration and vertical distribution of carbon dioxide in the stratosphere. *Nature* **316,** 708–710 (1985).
12. Foucher, P. Y. *et al.* Carbon dioxide atmospheric vertical profiles retrieved from space observation using ACE-FTS solar occultation instrument. *Atmos. Chem. Phys.* **11,** 2455–2470 (2011).
13. López-Puertas, M., Lopez-Valverde, M. A., Garcia, R. R. & Roble, R. G. in *Atmospheric Science Across the Stratopause* (eds Siskind, D. E. *et al.*) 83–100 (Geophys. Monog. Series, Vol. 123, American Geophysical Union, 2000).
14. Beagley, S. R. *et al.* First multi-year occultation observations of CO_2 in the MLT by ACE satellite: Observations and analysis using the extended CMAM. *Atmos. Chem. Phys.* **10,** 1133–1153 (2010).
15. Bernath, P. F. *et al.* Atmospheric Chemistry Experiment (ACE): Mission overview. *Geophys. Res. Lett.* **32,** L15S01 (2005).
16. Conway, T. J. *et al.* Evidence for interannual variability of the carbon cycle from the National Oceanic and Atmospheric Administration/Climate Monitoring and Diagnostics Laboratory Global Air Sampling Network. *J. Geophys Res.* **99,** 22831–22855 (1994).
17. Boone, C. D. *et al.* Retrievals for the atmospheric chemistry experiment Fourier-transform spectrometer. *Appl. Opt.* **44,** 7218–7231 (2005).
18. Qian, L., Roble, R. G., Solomon, S. C. & Kane, T. J. Calculated and observed climate change in the thermosphere, and a prediction for solar cycle 24. *Geophys. Res. Lett.* **33,** L23705 (2006).
19. Akmaev, R. A., Fomichev, V. I. & Zhu, X. Impact of middle-atmospheric composition changes on greenhouse cooling in the upper atmosphere. *J. Atmos. Solar-Terr. Phys.* **68,** 1879–1889 (2006).
20. Hoffmann, P., Rapp, M., Singer, W. & Keuer, D. Trends of mesospheric gravity waves at northern middle latitudes during summer. *J. Geophys Res.* **116,** D00P08 (2011).
21. Garcia, R. R., Randel, W. J. & Kinnison, D. E. On the determination of age of air trends from atmospheric trace species. *J. Atmos. Sci.* **68,** 139–154 (2011).
22. Emmert, J. T., Lean, J. L. & Picone, J. M. Record-low thermospheric density during the 2008 solar minimum. *Geophys. Res. Lett.* **37,** L12102 (2010).
23. American Institute of Aeronautics and Astronautics *Atmospheric Effects of Chemical Rocket Propulsion* (AIAA, 1991).
24. Isakowitz, S. J., Hopkins, J. P. Jr & Hopkins, J. B. *International Reference Guide to Space Launch Systems* 3rd edn (AIAA, 1999).
25. Emmert, J. T. & Picone, J. M. Statistical uncertainty of 1967–2005 thermospheric density trends derived from orbital drag. *J. Geophys. Res.* **116,** A00H09 (2011).

Acknowledgements

Author contributions

J.T.E. conceived the study, analysed the data and model output, and prepared the manuscript. M.H.S. and D.P.D. conducted the model simulations. M.H.S. calculated carbon emissions from space vehicle launches. P.F.B. and C.D.B. provided guidance on the use of the ACE-FTS retrievals. C.D.B. developed the ACE-FTS retrieval algorithms. All authors discussed the results, interpretations and implications, and contributed to the manuscript.

Additional information

Supplementary information is available in the online version of the paper. Reprints and permissions information is available online at www.nature.com/reprints. Correspondence and requests for materials should be addressed to J.T.E.

Competing financial interests

The authors declare no competing financial interests.